

The Global Energy Balance of Titan

Liming Li^{1*}, Conor A. Nixon², Richard K. Achterberg², Mark A. Smith¹, Nicolas J. P. Gorius²,
Xun Jiang¹, Barney J. Conrath³, Peter J. Gierasch³, Amy A. Simon-Miller⁴, F. Michael Flasar⁴,
Kevin H. Baines⁵, Andrew P. Ingersoll⁶, Robert A. West⁵, Ashwin R. Vasavada⁵,
Shawn P. Ewald⁶

¹ *Department of Earth and Atmospheric Sciences, University of Houston, Houston, TX 77204, USA.*

² *Department of Astronomy, University of Maryland, College Park, MD 20742, USA.*

³ *Department of Astronomy, Cornell University, Ithaca, NY 14853, USA.*

⁴ *NASA Goddard Space Flight Center, Greenbelt, MD 20771, USA.*

⁵ *Jet Propulsion Laboratory, Caltech, Pasadena, CA, 91109, USA.*

⁶ *Division of Geological and Planetary Sciences, Caltech, Pasadena, California, USA.*

To whom all correspondence should be addressed. E-mail: lli7@mail.uh.edu

Abstract: We report the first measurement of the global emitted power of Titan. Long-term (2004-2010) observations conducted by the Composite Infrared Spectrometer (CIRS) onboard Cassini reveal that the total emitted power by Titan is $(2.84 \pm 0.01) \times 10^8$ watts. Together with previous measurements of the global absorbed solar power of Titan, the CIRS measurements indicate that the global energy budget of Titan is in equilibrium within measurement error. The uncertainty in the absorbed solar energy places an upper limit on the energy imbalance of 5.3%.

The energy budget is a critical factor in determining the weather and climate on planets and satellites. Significant energy imbalance has been detected for the giant planets (1-5). The emitted thermal energy exceeds the absorbed solar energy by 57%, 80%, and 157% for Jupiter, Saturn, and Neptune, respectively (6-7). Such an energy imbalance is thought to be linked to the internal heat, which provides important clues to the understanding of planetary evolution and atmospheric circulation on the giant planets. On the other hand, Earth's global energy budget is in a near equilibrium state (8). A recent study (9) suggests that the global energy budget has a small imbalance with the absorbed solar energy exceeding the emitted thermal energy by just 0.4%. Even though the energy imbalance is very small, it has significant influences on global warming and climate changes on Earth (9). Titan, the biggest satellite of Saturn, is similar to Earth in many ways. Here, we explore a fundamental question: Is the global energy budget on Titan in an equilibrium state?

To evaluate the global energy budget of Titan, both the absorbed solar energy and the emitted thermal energy must be measured. The absorbed solar energy is determined by the bolometric Bond albedo with the known total solar radiance. The Bond albedo of Titan has already been measured based on observations by (1) Earth-based telescopes (10), (2) the imaging photopolarimeter onboard the Pioneer spacecraft (11), and (3) a combination of spacecraft and Earth-based telescopes (12). Even though these measurements were conducted at different times, the Bond albedo of Titan is approximately consistent between all three measurements.

Unfortunately, there are no direct measurements of the global emitted thermal radiance before the epoch of Cassini, mainly because of a lack of infrared observations with sufficient spectral range and spatial coverage. Due to the lack of the measurements of the global emitted radiance, the energy budget of Titan cannot be determined directly. An energy balance between the absorbed solar energy and the emitted thermal energy was simply assumed in previous studies of estimating Titan's effective temperature (10-12). On the other hand, some investigators (13-14) noted that the global energy budget of Titan could be imbalanced based on a simplified inversion model of Titan's atmosphere (15). Indeed, the computed energy imbalance of Titan reached as much as 38%, depending on the parameter setting of the inversion model (13-14). The inconsistency of above studies makes it important to measure the global emitted radiance of Titan. Such measurements provide not only information regarding Titan's thermal characteristics, but also constraints on its energy budget. Furthermore, any energy

balance/imbalance is probably relevant for climate change on Titan because such a relationship has already discovered on our own planet – Earth (9).

The direct computation of emitted power P_{emit} requires measurements of the spectral flux over a wide range of wavenumbers and emission angles (16-18). The Composite Infrared Spectrometer (CIRS) of Cassini (19) provides such measurements with nearly complete coverage of wavenumber and emission angle, which have not been conducted before. Figure 1 displays an example of a CIRS averaged spectrum of Titan. These are recorded by three focal planes (FP1, FP3, and FP4) with a total wavenumber coverage of 10-1430 cm^{-1} ($\sim 7\text{-}1000 \mu\text{m}$). Figure 1 shows that the radiance observed by FP1 is dominant in the total emitted power of Titan. Figure 1 also demonstrates emission/absorption bands in the stratosphere recorded by FP3 and FP4, which have relatively warmer brightness temperatures.

In order to precisely measure the total emitted power of Titan, we select a reference altitude, in which there is no downward thermal flux. At some latitudes of northern hemisphere, there is significant thermal emission up to nearly 500 km (20). Therefore, we set the reference altitude as 500 km in this study. In the CIRS data, the emission angle and latitude are referenced to the solid surface of Titan. The reference altitude of 500 km is a significant fraction of the solid body radius ~ 2575 km (21), so the variation with altitude of emission angle and latitude along a radiance ray cannot be ignored. We calculate a new emission angle and latitude at the reference altitude along the radiance ray path from the original CIRS emission angle and latitude as described in the Supporting Online Material.

All Titan spectra with two spectral resolutions (15.5 cm^{-1} and 2.8 cm^{-1}), which were recorded during the time period of 2004-2010, were used to compute the emitted power of Titan. The processing of the CIRS raw spectra is similar to the method used in our previous study of Saturn's emitted power (22). The final data produced are two-dimensional (latitude \times emission angle) matrices of wavenumber-integrated radiances of Titan with 1° resolution in both latitude and emission angle at the reference altitude of 500 km. Panel A of Fig. 2 is the final processed matrix, which displays Titan's spectrally-integrated radiance over the whole range (10-1430 cm^{-1}) of the three focal planes of CIRS (FP1, FP3, and FP4). This panel shows that the total radiance recorded by the three focal planes increases from 0° to $\sim 57^\circ$ along the direction of emission angle. When the emission angle at 500 km is less than $\sim 57^\circ$, the radiance recorded by FP3 and FP4 mainly comes from the stratosphere with temperature increasing with altitude. Therefore, the radiance recorded by FP3 and FP4 at high emission angles, which mainly comes from the relatively high and hence warm atmosphere, is significantly larger than the radiance at low emission angles, which comes from the relatively lower and hence colder stratosphere. In contrast, the radiance recorded by FP1, which mainly comes from the tropopause, does not vary significantly with emission angle. The variation of radiance recorded by FP3 and FP4 is dominant in the variation of total radiance shown in panel A when the emission angle is less than 57° . Panel A also shows that the total radiance decreases from $\sim 57^\circ$ to 90° along the direction of the emission angle. When the emission angle is larger than 57° at 500 km, the radiance shown in panel A comes from CIRS limb observations. For the limb observations, a radiance ray with high emission angle at 500 km has a significantly longer path in the upper stratosphere and mesosphere compared to a ray with a relatively low emission angle. The atmospheric density in the upper stratosphere and mesosphere decreases quickly with altitude, so the outgoing radiance

decreases with altitude in these regions. Therefore, the radiance recorded at high emission angles, which has greater contribution from the high and hence sparse atmosphere, is smaller than the radiance at low emission angles, which have more contribution from the lower, denser atmosphere for these limb observations.

Panel A of Fig. 2 also shows a few observational gaps at high emission angles and in the polar region. In order to enable numerical integration over the whole plane of emission angle and latitude, we use a least-square fit to interpolate/extrapolate from existing observations to fill observational gaps in Fig. 2, as described in our previous study of Saturn (22). After filling observational gaps in Fig.2, we then integrate the radiance over the direction of emission angle to get the emitted power at each latitude. The resulted emitted power is displayed in panel B of Fig. 2. The uncertainty shown in panel B is estimated by a combination of errors from (1) this procedure for filling observational gaps and (2) the calibration of CIRS spectra for removing the radiance of the background from the radiance of the target (19), which is discussed in our previous study (22). The meridional distribution of the emitted power shows a basic symmetry between two hemispheres even though they are in different seasons during the observational period of 2004-2010 (solar longitude from 293° to 5°; northern mid-winter to northern spring equinox). The radiative time constant of Titan's troposphere is probably longer than 100 Earth years (23), which explains why the seasonal signal does not show up in the meridional distribution of the emitted power. CIRS observations of the emitted power from pole to pole will benefit future investigations of the meridional distribution of Titan's energy balance.

The meridional distribution of the emitted power shown in Fig. 2 is further utilized to calculate the global average emitted power \bar{P}_{emit} (22, 24). The global average of the time-mean (2004-2010) of emitted power at the reference altitude (500 km) is 2.392 ± 0.010 watts/meter². The total emitted power can be computed by $P_{emit} = 4\pi(R_T + 500)^2 \bar{P}_{emit}$, where R_T is the solid body radius of Titan (2575 km). Therefore, Titan's emitted thermal power is $(2.84 \pm 0.01) \times 10^8$ watts.

The precise measurements of the emitted energy are important for the exploration of energy balance of Titan. When discussing the energy balance of Titan, we should consider thermal effects of Saturn and its rings besides the emitted power and absorbed solar radiance. Titan is $\sim 20 R_S$ (R_S is radius of Saturn) away from Saturn. The emitted power of Saturn decreases from $\sim 4.95 \text{ Wm}^{-2}$ at the surface (22) to $\sim 0.012 \text{ Wm}^{-2}$ at the distance of Titan, therefore the thermal effect of Saturn is inconsequential compared to the emitted power of Titan. Saturn's rings and Titan are in the same plane, so most thermal emissions from the inner rings will be blocked by outer rings. The outer rings have a very low temperature, so their thermal emissions have negligible effect on Titan. In summary, the thermal effect from Saturn and its rings will not affect the energy balance of Titan significantly. Therefore, the energy balance of Titan is mainly determined by the absorbed solar radiance and the emitted thermal radiance.

The solar constant at Titan is $15.2 \text{ watts/meter}^2$ (25). The variation of total solar irradiance is less than 0.1% between different solar cycles (26), which is neglected in our discussion of energy balance on Titan. The measurements of reflected solar radiance (10-12) suggest the average value of Bond albedo is 0.265 with an average uncertainty of Bond albedo of 0.03. The radius of the limb of Titan for the wavelength of Sun's peak radiation ($\sim 0.48 \mu\text{m}$) was

estimated as 2825 km (11, 27), which is basically consistent with recent studies based on radiation models (28-29). The total absorbed solar power can be expressed as $P_{absorb} = \pi R_L^2 I_S (1 - A)$, where R_L is the radius of limb of Titan at 0.48 μm , I_S is the solar constant at Titan, and A is the Bond albedo. Based on the known values of these parameters, we have the total absorbed solar power of Titan as $(2.80 \pm 0.11) \times 10^8$ watts.

Comparing the total absorbed solar power of $(2.80 \pm 0.11) \times 10^8$ watts with the total emitted thermal power of $(2.84 \pm 0.01) \times 10^8$ watts, we find that the global energy budget of Titan is in equilibrium within the measurement error of absorbed solar energy. The CIRS measurements of emitted energy are one-order of magnitude more precise than the previous measurements of the absorbed solar energy, so the primary uncertainty in determining the energy balance comes from the uncertainties of the absorbed solar radiance. We use the uncertainties of absorbed solar radiance to estimate the upper limit of the possible energy imbalance. The range of absorbed solar energy is from 2.69×10^8 joules to 2.91×10^8 joule, which suggests that the difference between the absorbed solar energy and the emitted thermal energy varies from -5.3% $((2.69 - 2.84) / 2.84 \sim -5.3\%)$ to 2.5% $((2.91 - 2.84) / 2.84 \sim 2.5\%)$. Therefore, the possible energy imbalance cannot exceed 5.3%, which excludes the possibility of large energy imbalance on Titan in the previous studies (13-14).

Our analyses suggest a basic equilibrium of global energy budget on Titan, but we cannot rule out the possibility of a small energy imbalance on the satellite due to the relatively large uncertainty of the Bond albedo in the previous measurements. It is possible to obtain more precise measurements of the Bond albedo based on observations from the Cassini ISS and VIMS instruments. The wavelengths of ISS (0.26-1.0 μm) and VIMS (0.35-5.1 μm) occupy nearly the complete spectral range of solar radiance. With a good coverage of phase angle by the extensive observations of Cassini during the period of 2004-2010, the reflected radiance recorded by the two instruments (ISS and VIMS) can be utilized to measure the Bond albedo of Titan at a much better precision than before. In addition, the long-term global observations conducted by Cassini make it possible to study the variation of energy budget in space and time (e.g., seasonally), which will provide one more perspective of investigating the climate changes on Titan in addition to the greenhouse and anti-greenhouse effects (30).

References and Notes

1. A. P. Ingersoll, G. Munch, G. Neugebauer, D. J. Dineer, G. S. Orton, B. Schupler, M. Schroeder, S. C. Chase, R. D. Ruiz, L. M. Trafton, *Science* **188**, 472 (1975).
2. G. S. Orton, A. P. Ingersoll, *J. Geophys. Res.* **85**, 5871 (1980).
3. R. A. Hanel, B. J. Conrath, L. W. Herath, V. G. Kunde, J. A. Pirraglia, *J. Geophys. Res.* **86**, 8575 (1981).
4. Hanel, R. A., B. J. Conrath, V. G. Kunde, J. C. Pearl, J. A. Pirraglia, *Icarus* **53**, 262 (1983).
5. J. C. Pearl, R. A. Hanel, J. A. Pirraglia, *Icarus* **84**, 12 (1990).
6. B. J. Conrath, R. A. Hanel, R. E. Samuelson, in *Origin and Evolution of Planetary and Satellite Atmospheres*, S. K. Atreya, J. B. Pollack, M. S. Matthews, Eds. (Univ. of Arizona Press, Arizona, 1989).
7. A. P. Ingersoll, *Science* **20**, 308 (1990).
8. K. E. Trenberth, J. T. Fasullo, J. Kiehl, *Bull. Amer. Meteor. Soc.* **90**, 311 (2009).
9. J. Hansen *et al.*, *Science* **308**, 1431 (2005).
10. R. L. Younkin, *Icarus* **21**, 219 (1974).
11. M. G. Tomasko, P. H. Smith, *Icarus* **51**, 65 (1982).
12. J. S. Neff, T. A. Ellis, J. Apt, J. T. Bergstralh, *Icarus* **62**, 425 (1985).
13. F. J. Low, G. H. Rieke, *Astrophys. J.* **190**, 143 (1974).
14. J. Caldwell, in *Planetary Satellites*, Burns, J. A., Eds. (Univ. of Arizona Press, Arizona, 1989).
15. R. E. Danielson, J. J. Caldwell, D. R. Larach, *Icarus* **20**, 437 (1973).
16. S. Chandrasekhar, *Radiative Transfer* (Oxford Univ. Press, New York, 1950).
17. R. M. Goody, Y. L. Yung, *Atmospheric Radiation: Theoretical Basis* (Oxford Univ. Press, New York, 1989).
18. R. A. Hanel, B. J. Conrath, D. E. Jennings, R. E. Samuelson, *Exploration of the solar system by Infrared Remote Sensing* (Cambridge Univ. Press, New York, 2003).
19. F. M. Flasar *et al.*, *Space Sci. Rev.* **115**, 169 (2004).
20. R. K. Achterberg, B. J. Conrath, P. J. Gierasch, F. M. Flasar, C. A. Nixon, *Icarus* **194**, 263 (2008).
21. H. A. Zebker, B. Stiles, S. Hansley, R. Lorenz, R. L. Kirk, J. Lunine, *Science* **324**, 921 (2009).
22. L. Li *et al.*, *J. Geophys. Res.* **115**, E11002 (2010).
23. F. M. Flasar, R. E. Samuelson, B. J. Conrath, *Nature* **292**, 693 (1981).
24. A. P. Ingersoll *et al.*, *Science* **188**, 472 (1975).
25. R. E. Samuelson, *Icarus* **53**, 364 (1983).
26. R. C. Willson, A. V. Mordvinov, *Geophys. Res. Lett.* **30**, 1199 (2003).
27. P. H. Smith, *J. Geophys. Res.* **85**, 5943 (1980).
28. C. P. McKay, J. B. Pollack, R. Courtin, *Icarus* **80**, 23 (1989).
29. M. G. Tomasko, B. Bezard, L. Dose, S. Engel, E. Karkoschka, S. Vinatier, *Planetary and Space Science* **56**, 648 (2008).
30. C. P. McKay, J. B. Pollack, R. Courtin, *Science* **253**, 1118 (1991).

Acknowledgements: This work was supported by NASA Outer Planets Research Program.

Figure Captions

Figure 1. Combined spectral radiance from the three spectral ranges covered by FP1, FP3, and FP4. The combined spectrum has wavenumber ranges $10\text{-}557\text{ cm}^{-1}$, $575\text{-}1050\text{ cm}^{-1}$, and $1055\text{-}1430\text{ cm}^{-1}$, for FP1, FP3, and FP4, respectively. The example shown in Fig. 1, which was recorded at a spectral resolution of 2.8 cm^{-1} , is an average of spectra over the whole year of 2007 with a latitude range of $30^{\circ}\text{N}\text{-}30^{\circ}\text{S}$ and emission angle range of $0\text{-}30^{\circ}$ at an altitude of 500 km. (A) CIRS radiance. (B) Corresponding brightness temperature.

Figure 2. Coverage of CIRS observations and the emitted power of Titan at the reference altitude of 500 km. (A) Time mean (2004-2010) wavenumber-integrated radiance in the plane of latitude and emission angle. The wavenumber-integrated radiance in panel A is a combination of the three focal planes (FP1, FP3, and FP4) over the spectral range of $10\text{-}1430\text{ cm}^{-1}$. The radiance with emission angle less than 57° at the altitude of 500 km comes from CIRS nadir observations, and the radiance with emission angle larger than 57° comes from CIRS limb observations. All CIRS observations of Saturn's atmosphere with two spectral resolutions (15.5 cm^{-1} 2.8 cm^{-1}) between October 2004 and March 2010 are averaged to the temporal mean radiance in panel A. CIRS observations with other spectral resolutions, which have negligible spatial coverage, are not included in this study. (B) Meridional distribution of the emitted power. The thick line is the profile of the emitted power and vertical lines represent the uncertainties. The estimated uncertainty is combined by the uncertainty related to the filling observational gaps and the uncertainty related to the calibration.

Figure 1

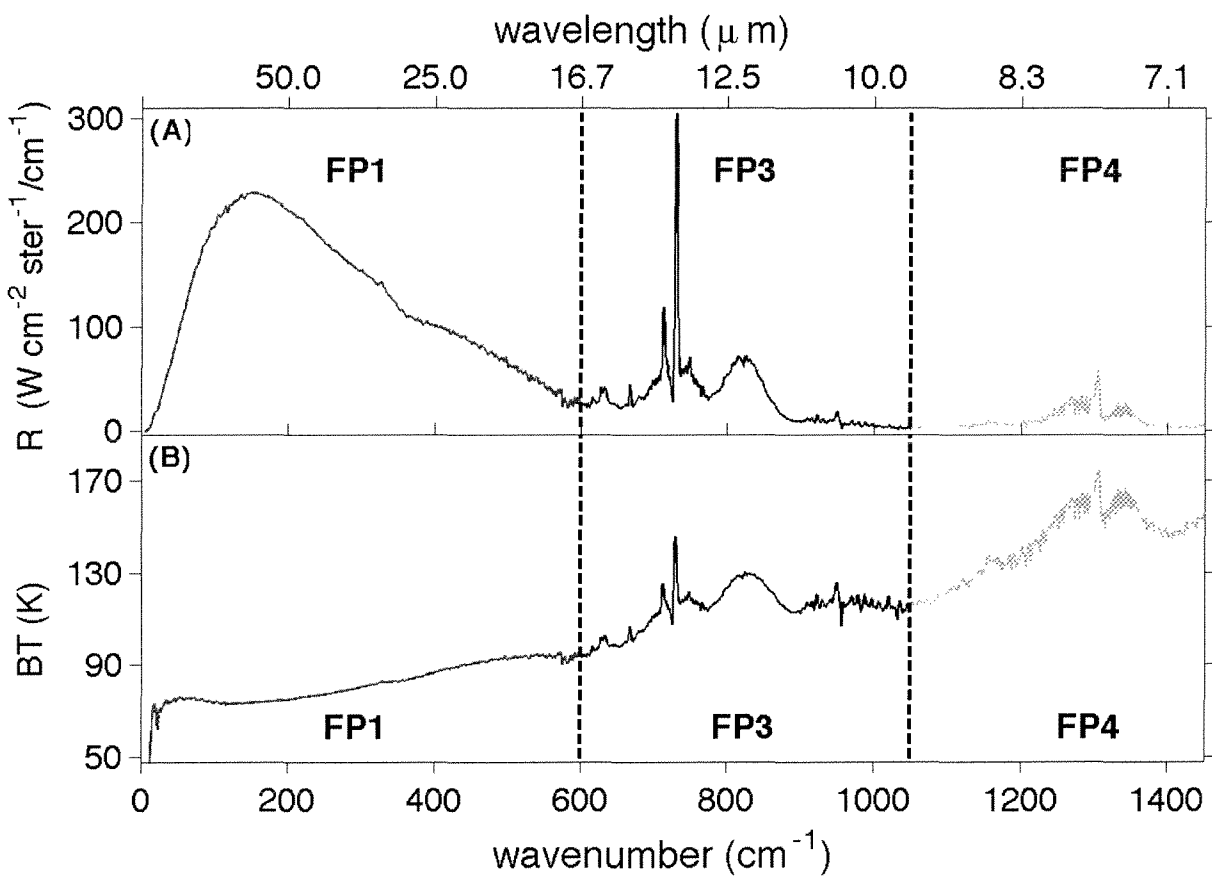
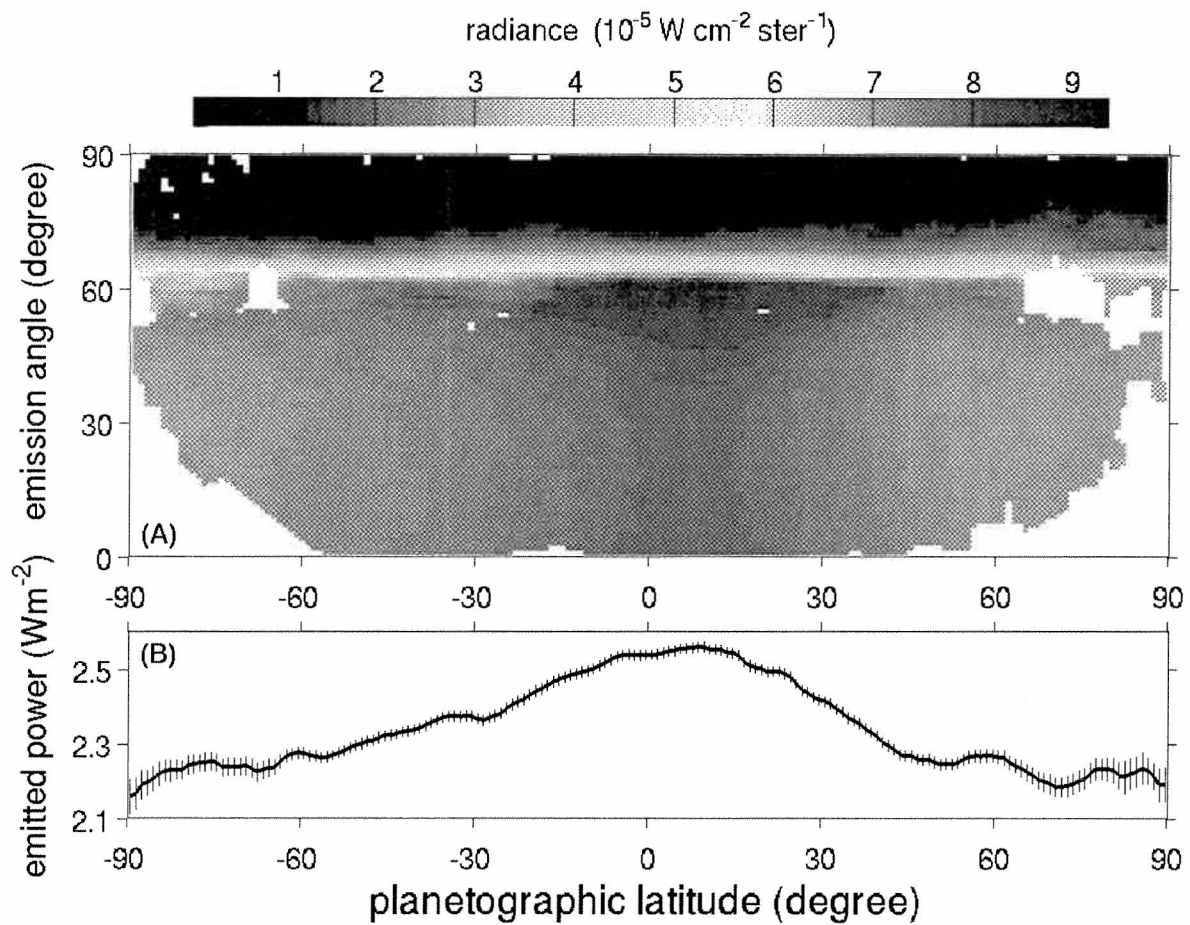


Figure 2



Supporting Online Material for The Global Energy Balance of Titan

Liming Li^{1*}, Conor A. Nixon², Richard K. Achterberg², Mark A. Smith¹, Nicolas J. P. Gorius²,
Xun Jiang¹, Barney J. Conrath³, Peter J. Gierasch³, Amy A. Simon-Miller⁴, F. Michael Flasar⁴,
Kevin H. Baines⁵, Andrew P. Ingersoll⁶, Robert A. West⁵, Ashwin R. Vasavada⁵,
Shawn P. Ewald⁶

¹ Department of Earth and Atmospheric Sciences, University of Houston, Houston, TX 77204, USA.

² Department of Astronomy, University of Maryland, College Park, MD 20742, USA.

³ Department of Astronomy, Cornell University, Ithaca, NY 14853, USA.

⁴ NASA Goddard Space Flight Center, Greenbelt, MD 20771, USA.

⁵ Jet Propulsion Laboratory, Caltech, Pasadena, CA, 91109, USA.

⁶ Division of Geological and Planetary Sciences, Caltech, Pasadena, California, USA.

Calculation of Emission Angle and Latitude At the Reference Altitude

We introduce the geometry to compute the new emission angle and latitude at the reference altitude of 500 km from the original CIRS emission angle and altitude, which are referenced to the solid surface of Titan. Figure S1 shows that the original emission angle on the solid surface and the new emission angle on the sphere at the reference altitude.

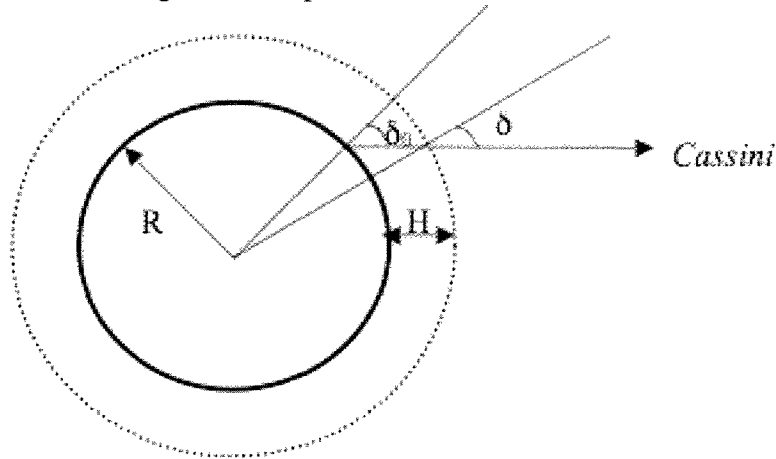


Figure S1. Conversion of the emission angle between the solid surface and the reference altitude for the CIRS nadir observations.

In Fig. S1, the reference altitude (500 km) and the solid body radius of Titan (2575 km) are represented by H and R , respectively. In addition, we represent the original emission angle at the solid surface and the new emission angle at the reference altitude by δ_0 and δ , respectively. Based on the geometry shown in Fig. S1, we have the conversion between the original emission angle and the new emission angle as below.

$$\frac{R+H}{\sin \delta_0} = \frac{R}{\sin \delta} \Rightarrow \delta = \arcsin\left(\frac{R \sin \delta_0}{R+H}\right) \quad (1)$$

The above conversion works for the CIRS nadir radiance. For nadir observations, we found that the range of the new emission angle δ is from 0° to $\sim 57^\circ$ at the altitude of 500 km, which shrinks from the range of 0° - 90° for the original emission angle at the surface. Equation (1) shows that the new emission angle δ is less than the original latitude δ_0 due to the factor $R/(R+H) < 1$, which results in the shrinking of the range of the new emission angle. In order to fill the gaps of 57° - 90° in the new emission angle, we include CIRS limb observations into this study.

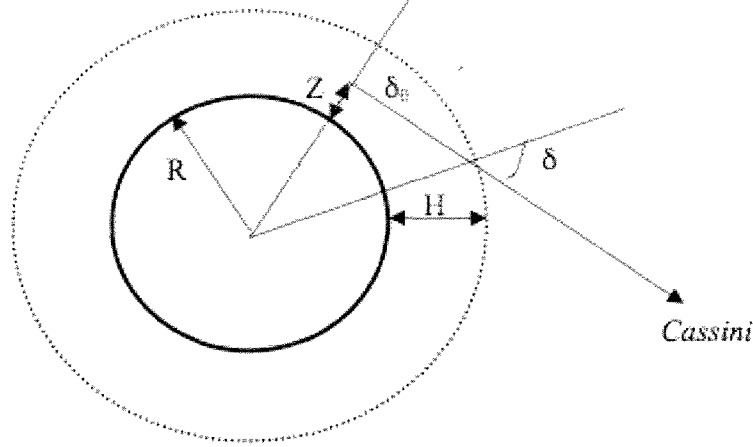


Figure S2. Conversion of the emission angle between the solid surface and the reference altitude for the CIRS limb observations.

Figure S2 shows the original emission angle and the new emission angle for a limb observation. The limb radiance ray is tangent of the sphere at the altitude Z , so the original emission angle δ_0 at the altitude Z is a right angle. The new emission angle δ , which is referenced to the sphere at the reference altitude H , can be expressed as

$$\sin \delta = \frac{R+Z}{R+H} \Rightarrow \delta = \arcsin\left(\frac{R+Z}{R+H}\right) \quad (2)$$

The conversion of emission angle between the solid surface and the reference altitude is straightforward, so we have the simple relationship shown in the equations (1) and (2). The conversion of latitude between the solid surface and the reference altitude is relatively complicated. We do not have the simple geometry for this conversion. For the CIRS nadir observations, we use a method of parameterization to compute the new latitude at the sphere of the reference altitude, which is outlined as three steps: i) Define the observational location at the surface and the spacecraft's location in sphere coordinates; ii) Parameterize a line to connect the two locations, which represents the ray path originating from the observational location at the surface; and iii) Solve the ray path for where it intersects the reference altitude (500 km) to get the new location (latitude and longitude) at the reference altitude. The parameterization of ray paths also works for the CIRS limb observations except for setting the sphere at the tangent heights as the new surface.